Modeling the effect of multiple sets of mesoscale fractures in porous rock on frequency-dependent anisotropy

GEOPHYSICS, VOL. 74, NO. 6 (NOVEMBER-DECEMBER 2009); P. D97–D103, 4 FIGS.
10.1190/1.3204779

Modeling the effect of multiple sets of mesoscale fractures in porous rock on frequency-dependent anisotropy

Mark Chapman[1]

ABSTRACT

This study models the seismic response of porous rock containing two fracture sets with different orientations, sizes, and connectivities. Modeling demonstrates frequency-dependent anisotropy controlled by two characteristic frequencies that are defined by fluid mobility and the length scales of the fractures. Fracture-related dispersion and attenuation typically occur over a wider frequency band than is seen in the case of a single fracture set. When one set of fractures is modeled as being sealed, the azimuthal variation of velocity and attenuation can be different, with the azimuth of minimum attenuation coinciding with the strike direction of the open fracture set. The results should support attempts to differentiate between open and closed fractures on the basis of seismic measurements.

INTRODUCTION

Analysis of field data (Maultzsch et al., 2007a) suggests that consideration of the frequency dependence of seismic anisotropy potentially can give access to fluid-saturation and fracture-scale information in fractured reservoirs. Attempts to extract this information from the data depend on the availability of suitable theoretical models. Unfortunately, current theoretical models have significant limitations.

Frequency dependence of seismic velocity and attenuation often is associated with the concept of fluid mobility (Batzle et al., 2006) because the wave-induced exchange of fluid between different parts of the pore space is believed to be a driving mechanism behind frequency dependence. In the anisotropic case, the influence of fractures in this process is studied by Hudson et al. (1996), Pointer et al. (2000), van der Kolk et al. (2001), and Jakobsen (2004), among others. Chapman (2003) establishes the link between this behavior and the scale length of the fractures, but the model is limited to a single set of fractures larger than the grain scale. The need to consider more complex fracture distributions within the model is recognized (Barton, 2007).

I present a technique to extend earlier analysis (Chapman, 2003) to the case of two sets of fractures with different scale lengths and orientations. I work to the first order in the fracture number density. The method is in two parts. First, I define a system of equations that describes the flow of fluid between cracks and pores in response to a passing seismic wave. Second, I use the solution of this system to compute the elastic corrections resulting from the presence of such fluid-communicating fractures. The analysis results in a complex-valued, frequency-dependent anisotropic elastic tensor.

Behavior is dominated by the existence of two characteristic timescales, corresponding to the two length scales of the fracture sets. For the case of an open set and a closed set of fractures, important differences are predicted between the velocity anisotropy and the attenuation anisotropy. My goal is that the results of this paper can be used to improve inferences about the azimuthal variation of permeability in fractured reservoirs.

THEORY

Let us consider the case of a fracture surrounded by spherical pores. The fracture is modeled as a circular ellipsoid of small aspect ratio. Stress is applied to the system, and a different pressure is induced in the fracture compared to the pores as a result of a difference in geometry. This pressure difference is to be relieved by fluid flow.

We base our analysis on the Darcy equation:

$$dQ = \frac{k}{\eta} dS \cdot \nabla p, \tag{1}$$

which relates the fluid mass flux dQ through a surface dS to the pressure gradient ∇p and fluid mobility parameter k/η, the ratio of permeability to fluid viscosity.

Consider the case in which two inclusions are adjacent to each other, containing fluid at pressures p_1 and p_2, respectively. To apply the Darcy equation, we assume

Manuscript received by the Editor 2 April 2008; revised manuscript received 30 October 2008; published online 14 October 2009.
[1]British Geological Survey, Edinburgh Anisotropy Project, Edinburgh, U. K. E-mail: m.chapman@bgs.ac.uk.

$$\nabla p \cdot dS = \frac{p_2 - p_1}{\ell} a^2, \tag{2}$$

in which ℓ has the sense of a separation between the adjacent intergranular voids and a has the sense of a cross section of area through which fluid flows. This leads to the flow law between an inclusion and its neighbor:

$$\partial_t m_1 = \frac{\rho_f^0 k a^2}{\eta}(p_2 - p_1), \tag{3}$$

where m_1 is the fluid mass in the first void and ρ_f^0 is the unstressed fluid density. Chapman et al. (2002) implicitly write

$$\varsigma = \frac{a^2}{\ell} \tag{4}$$

as the length scale controlling the fluid flow. They further suggest that this scale length should be associated with the grain size because that is the only assumed length scale in the model.

We model inclusions that communicate with more than one neighbor by assuming that the flows can be added linearly and by introducing a coordination number C:

$$\partial_t m_i = \frac{C \rho_f k \varsigma}{\eta}(p_j - p_i). \tag{5}$$

This framework can be adapted to model the case of a large fracture surrounded by smaller pores. We think of the fluid mass flow from the fracture as an integral over the fracture surface, which may be written formally as

$$\partial_t m_f = \rho_f \oint\!\!\oint_S dQ = \rho_f \oint\!\!\oint_S \frac{k}{\eta}(dS . \nabla p). \tag{6}$$

This integral can be replaced by a sum of a certain number of individual interactions between the fracture and the surrounding pores. We can further assume homogeneous conditions on the fracture surface, written as

$$\partial_t m_f = \frac{\rho_f^0 k a_f^2}{\eta \ell}(p^* - f), \tag{7}$$

in which p^* denotes the pressure in the spherical pores and f denotes the fluid pressure in the fracture.

Consistency between the single-scale and multiscale theories is achieved through the formal condition

$$\lim_{a_f \to \varsigma} \frac{a_f^2}{\ell \varsigma} = C. \tag{8}$$

We now solve the system of equations, calculating the pressures as a function of the applied stress in the frequency domain. Following Chapman et al. (2002), we can write the volume of the fracture as a function of applied normal stress and fluid pressure:

$$V_f = V_f^0\left(1 - \frac{\sigma_n}{\sigma_c} + \frac{f}{\sigma_c}\right), \tag{9}$$

in which we write (Eshelby, 1957)

$$\sigma_c = \frac{\pi \mu r}{2(1 - \upsilon)}, \tag{10}$$

where r is the aspect ratio of the crack, υ is Poisson's ratio, and λ and μ are the Lamé parameters of the background medium throughout. In this equation, σ_n is the normal stress acting on the crack face. We assume a relation between fluid density and pressure:

$$\rho_f = \frac{\rho_f^0}{1 - \dfrac{p}{\kappa_f}}, \tag{11}$$

where κ_f is the fluid bulk modulus. This allows us to couple the mass flow out of the fracture to the derivatives of fluid pressure and applied stress:

$$\partial_t m_f = \frac{m_f^0}{\sigma_c}[(1 + K_c)\partial_t f - \partial_t \sigma_n], \tag{12}$$

where

$$m_f^0 = \frac{4}{3}\pi a_f^3 r \rho_f^0, \tag{13}$$

$$K_c = \frac{\sigma_c}{\kappa_f}, \tag{14}$$

and a_f is the fracture radius. Then, we define a timescale τ_f:

$$\tau_f = \frac{8\ell(1 - \upsilon)(1 + K_c)}{3\mu}\left(\frac{\eta}{k}\right)a_f. \tag{15}$$

Our equation coupling the fracture pressure to that in the surrounding pores is given in the frequency domain by

$$f = \frac{i\omega\tau_f}{1 + i\omega\tau_f}\frac{\sigma_n}{1 + K_c} + \frac{p^*}{1 + i\omega\tau_f}. \tag{16}$$

Having developed the equations for the case of a single fracture surrounded by spherical pores, we proceed to the case in which we have multiple fracture sets embedded in a matrix whose porosity consists of such spherical pores. To solve this problem in a fully rigorous manner, we would have to specify the relative positions of each fracture set and compute an extremely complex spatially varying pore-fluid pressure field in the micropores.

Such considerations do not apply in the low- or high-frequency limiting cases, studied as a special case by Chapman et al. (2002). When we consider such solutions for very thin cracks, it is striking that the resultant fluid pressures in the pores are very similar in both limits but the fracture-fluid pressures are markedly different. To a reasonable approximation, we may believe the pressure in the fractures falls to that in the pores while the pore pressure remains roughly constant. This is understandable because the fractures contain little fluid but are highly compliant. When a small amount of fluid is transferred from the fracture to a pore, the results is a large drop in the fracture pressure, but there is a much smaller increase in the pore pressure because of smaller compliance of the pore.

We therefore ignore the complex spatial variations in pore pressure and consider pressure fields that vary as a function of time but not space. With this assumption, we have the system of equations

$$\partial_t m_f^1 = \frac{\rho_f^0 k a_1^2}{\eta \ell}(p^* - f_1), \tag{17}$$

$$\partial_t m_f^2 = \frac{\rho_f^0 k a_2^2}{\eta \ell}(p^* - f_2), \tag{18}$$

and

$$\partial_t m_f^1 + \partial_t m_f^2 + \partial_t m_p = 0, \tag{19}$$

in which equation 19 is a statement of conservation of pore-fluid mass. The superscript denotes the number of the fracture set to which the relevant variable refers. We have two different fracture radii, so, following equation 15, we have two different τ_f values, denoted τ_1 and τ_2.

We know how to write the fluid mass in a pore as a function of the applied stress and pore pressure (Chapman et al., 2002):

$$\partial_t m_p = \frac{3m_p^0}{4\mu}\left[(1+K_p)\partial_t p^* - \frac{1-v}{1+v}\partial_t \sigma_{ll}\right], \tag{20}$$

$$K_p = \frac{4\mu}{3\kappa_f}. \tag{21}$$

We can solve this system for the fluid pressure in each element as a function of the applied stress.

We first define the notation:

$$S_{ij}^1(\omega) = \frac{i\omega\tau_1 n_i^1 n_j^1}{(1+i\omega\tau_1)(1+K_c^1)} \tag{22}$$

and

$$S_{ij}^2(\omega) = \frac{i\omega\tau_2 n_i^2 n_j^2}{(1+i\omega\tau_2)(1+K_c^2)}, \tag{23}$$

in which n is the component of the unit normal vector to the fracture surface. We also define

$$F_1(\omega) = \frac{1}{1+i\omega\tau_1} \tag{24}$$

and

$$F_2(\omega) = \frac{1}{1+i\omega\tau_2}. \tag{25}$$

With this arrangement, the fluid pressure in the pores may be given by

$$\tilde{p}^* = H_{ij}^3(\omega)\tilde{\sigma}_{ij}, \tag{26}$$

in which

$$H_{ij}^3(\omega) = \frac{\frac{\varphi_1^0}{\sigma_c^1}[n_i^1 n_j^1 - (1+K_c^1)S_{ij}^1(\omega)] + \frac{\varphi_2^0}{\sigma_c^2}[n_i^2 n_j^2 - (1+K_c^2)S_{ij}^2(\omega)] + \frac{3\varphi_p^0}{4\mu}\frac{1-v}{1+v}\delta_{ij}}{\frac{\varphi_1^0}{\sigma_c^1}(1+K_c^1)F_1(\omega) + \frac{\varphi_2^0}{\sigma_c^2}(1+K_c^2)F_2(\omega) + \frac{3\varphi_p^0}{4\mu}(1+K_p)} \tag{27}$$

and ϕ denotes the volume fraction of the pores or fracture set, as defined by the subscript. Likewise, the pressures in the two fracture sets are found to be

$$\tilde{f}_1 = H_{ij}^1(\omega)\tilde{\sigma}_{ij} \tag{28}$$

and

$$\tilde{f}_2 = H_{ij}^2(\omega)\tilde{\sigma}_{ij}, \tag{29}$$

where we define

$$H_{ij}^1(\omega) = S_{ij}^1(\omega) + F_1(\omega)H_{ij}^3(\omega) \tag{30}$$

and

$$H_{ij}^2(\omega) = S_{ij}^2(\omega) + F_2(\omega)H_{ij}^3(\omega). \tag{31}$$

Chapman (2003) calculates the frequency-dependent effective elastic tensor using the formula (Eshelby, 1957)

$$C_{ijk\ell}\varepsilon_{ij}^0\varepsilon_{k\ell}^0 = C_{ijk\ell}^m\varepsilon_{ij}^0\varepsilon_{k\ell}^0 - \sum_n \varphi_n(\varepsilon_{ij}^{\text{inc}}\sigma_{ij}^0 - \sigma_{ij}^{\text{inc}}\varepsilon_{ij}^0), \tag{32}$$

relating the effective elastic tensor to that of the background medium through arbitrary elastic fields at infinity superscript zero, which induce elastic fields with the superscript "inc" (for inclusions) inside each void. This approach assumes a dilute concentration of inclusions so that the solution for the deformation of a single crack or pore in an infinite medium in response to stress and strain applied far from the crack can be used. The procedure adopted in that study (Chapman, 2003) was to choose particular values of the applied stress σ^0 and strain ε^0 with respect to the fracture orientation to isolate the five independent components of the elastic tensor, one by one. In the current case, we must extend this technique to handle the case where the resulting effective elastic tensor can have a much more complex form.

Our frequency-dependent effective elastic tensor will have the form

$$C_{ijk\ell}(\omega) = C_{ijk\ell}^0 - \phi C_{ijk\ell}^p(\omega) - \varepsilon_1 C_{ijk\ell}^{f1}(\omega) - \varepsilon_2 C_{ijk\ell}^{f2}(\omega), \tag{33}$$

in which the first correction is the isotropic elastic tensor for the background medium, the second correction is the isotropic elastic tensor associated with the spherical pores, and the last two corrections correspond to the fractures. The fracture corrections are proportional to the relevant fracture densities. The tensors for the fracture corrections are transversely isotropic (TI), but they only take the familiar simplified form of the TI tensor when they are referred to a

system of coordinates in which one of the axes is parallel to the fracture strike; more complex representations generally are expected in the material coordinate system.

If no fluid exchange were allowed between the cracks and pores, then each crack correction $C^{fn}_{ijk\ell}(\omega)$ in equation 33 would only contain information about the geometry of its respective crack set. When fluid exchange is allowed, the crack corrections contain information about the geometry of every crack and pore in the system. This dependence arises through the pore-fluid pressure field and is implicit in equations 28 and 29. In what follows, we derive explicit equations for $C^{fn}_{ijk\ell}(\omega)$ using equations 28 and 29.

We work to the first order in the porosity and fracture densities, and we ignore the elastic interactions between the cracks and pores. The procedure is to apply the appropriate elastic fields at infinity to isolate the various elastic constants in the local coordinate system for each crack, rotating the fields into the material frame to calculate the appropriate pressures. We then rotate the appropriately constructed crack corrections back into the material coordinate system and add the corrections linearly.

We define orientation angles θ_m and φ_m such that the mth crack set has a normal direction:

$$\underline{n}^m = (\cos\,\theta_m \sin\,\varphi_m, \sin\,\theta_m \sin\,\varphi_m, \cos\,\varphi_m). \tag{34}$$

In terms of these angles, we define a rotation matrix:

$$R^m_{ij}(\theta_m,\varphi_m) = \begin{bmatrix} \cos\,\theta_m \cos\,\varphi_m & -\sin\,\theta_m & \cos\,\theta_m \sin\,\varphi_m \\ \sin\,\theta_m \cos\,\varphi_m & \cos\,\theta_m & \sin\,\theta_m \sin\,\varphi_m \\ -\sin\,\phi_m & 0 & \cos\,\varphi_m \end{bmatrix}. \tag{35}$$

We first define the set of applied stress tensors:

$$\sigma^1_{ij} = \begin{bmatrix} \lambda+2\mu & 0 & 0 \\ 0 & \lambda & 0 \\ 0 & 0 & \lambda \end{bmatrix}, \tag{36}$$

$$\sigma^2_{ij} = \begin{bmatrix} \lambda & 0 & 0 \\ 0 & \lambda & 0 \\ 0 & 0 & \lambda+2\mu \end{bmatrix}, \tag{37}$$

$$\sigma^3_{ij} = \begin{bmatrix} 2(\lambda+\mu) & 0 & 0 \\ 0 & 2(\lambda+\mu) & 0 \\ 0 & 0 & 2\lambda \end{bmatrix}, \tag{38}$$

and

$$\sigma^4_{ij} = \begin{bmatrix} 2(\lambda+\mu) & 0 & 0 \\ 0 & 2\lambda & 0 \\ 0 & 0 & 2(\lambda+\mu) \end{bmatrix}. \tag{39}$$

Each of these tensors is used as the stress field at infinity σ^0_{ij} in equation 32. Their forms are chosen to isolate the various components of the resulting fracture correction tensors easily.

Corresponding to each of these stress tensors, we define a set of fluid pressures according to

$$f^p_m = H^m_{ij} R^m_{ia} R^m_{jb} \sigma^p_{ab}. \tag{40}$$

These fluid pressures then are used to define the elastic corrections, following equation 32:

$$a^m_{11} = \varphi^0_m \left[\frac{\lambda}{\sigma^m_c}(\lambda - f^1_m) - f^1_m \right], \tag{41}$$

$$a^m_{33} = \varphi^0_m \left[\frac{\lambda+2\mu}{\sigma^m_c}(\lambda+2\mu - f^2_m) - f^2_m \right], \tag{42}$$

$$a^m_{12} = \varphi^0_m \left[\frac{\lambda}{\sigma^m_c}(2\lambda - f^3_m) - f^3_m \right] - \frac{1}{2}(a^m_{11} + a^m_{33}), \tag{43}$$

$$a^m_{13} = \varphi^0_m \left[\frac{\lambda+\mu}{\sigma^m_c}(2\lambda+2\mu - f^4_m) - f^4_m \right] - \frac{1}{2}(a^m_{11} + a^m_{33}), \tag{44}$$

and

$$a^m_{55} = \phi^0_m \frac{4\mu(1-v)}{\pi(2-v)r_m}. \tag{45}$$

We then define the tensors $a^m_{ijk\ell}$ in standard matrix form as

$$\begin{bmatrix} a^m_{11} & a^m_{12} & a^m_{13} & 0 & 0 & 0 \\ a^m_{12} & a^m_{11} & a^m_{13} & 0 & 0 & 0 \\ a^m_{13} & a^m_{13} & a^m_{33} & 0 & 0 & 0 \\ 0 & 0 & 0 & a^m_{55} & 0 & 0 \\ 0 & 0 & 0 & 0 & a^m_{55} & 0 \\ 0 & 0 & 0 & 0 & 0 & 0 \end{bmatrix}. \tag{46}$$

We repeat this analysis for the corrections because of the presence of the pores. We begin by defining the applied stress tensor:

$$\sigma^5_{ij} = \begin{bmatrix} 3\lambda+2\mu & 0 & 0 \\ 0 & 3\lambda+2\mu & 0 \\ 0 & 0 & 3\lambda+2\mu \end{bmatrix}. \tag{47}$$

Then we define the pore-fluid pressure:

$$p^* = H^3_{ij} \sigma^5_{ij}. \tag{48}$$

In terms of these parameters, we write the elastic corrections:

$$d = \varphi \left[\frac{3\lambda+4\mu}{12\mu} \left(\frac{1-v}{1+v} \sigma^5_{\ell\ell} - p^* \right) - \frac{1}{3} p^* \right] \tag{49}$$

and

$$e = \phi 15\mu \frac{1-v}{7-5v}. \tag{50}$$

Based on these calculations, we can define the elastic correction tensor for the presence of the pores $C^p_{ijk\ell}(\omega)$ in standard matrix form as

$$\begin{bmatrix} \left(d+\frac{4}{3}e\right) & \left(d-\frac{2}{3}e\right) & \left(d-\frac{2}{3}e\right) & 0 & 0 & 0 \\ \left(d-\frac{2}{3}e\right) & \left(d+\frac{4}{3}e\right) & \left(d-\frac{2}{3}e\right) & 0 & 0 & 0 \\ \left(d-\frac{2}{3}e\right) & \left(d-\frac{2}{3}e\right) & \left(d+\frac{4}{3}e\right) & 0 & 0 & 0 \\ 0 & 0 & 0 & e & 0 & 0 \\ 0 & 0 & 0 & 0 & e & 0 \\ 0 & 0 & 0 & 0 & 0 & e \end{bmatrix}. \quad (51)$$

The overall effective, frequency-dependent elastic tensor is given as a sum of the background tensor, the porosity correction, and the two fracture corrections rotated into the material coordinate system:

$$C_{ijk\ell}(\omega) = C^0_{ijk\ell} - C^p_{ijk\ell}(w) - \sum_{m=1}^{2} R^m_{ip} R^m_{jq} R^m_{kr} R^m_{\ell s} a^m_{pqrs}. \quad (52)$$

NUMERICAL RESULTS

We now perform some numerical calculations to illustrate the predictions of the model. For the background elastic parameters, we take $\lambda = 51$ GPa and $\mu = 29$ GPa to simulate the properties of calcite. The density is 2.71 g/cm^3, and porosity is 8%. The saturating fluid is taken to be water. Following the analysis of Chapman (2003), we assume that a fracture radius of 1 m is associated with a τ_f value of 0.1 s.

We consider the case where we have two fracture sets, each with a fracture density of 0.02 and aspect ratio of 0.0001. When the orientations and sizes of the two sets are the same, we have a result consistent with that of Chapman (2003), where the fracture density is 0.04. Figure 1 shows the predicted P-wave velocity as a function of frequency for propagation 30° from the vertical and fracture strike directions when the fracture radius is 10 cm. Figure 2 shows the effect of repeating the calculation with one of the fracture radii set to 5 mm. One of the characteristic timescales is therefore decreased; the transition frequency becomes higher, and the dispersion occurs over a wider frequency band. The low- and high-frequency limits of velocity remain unchanged.

We next consider the case where we again have two fracture sets with a radius of 10 cm; this time, the fractures are vertical but the strike direction is 90° for one set and 130° for the other. Figure 3 shows the azimuthal variation of P-wave velocity and attenuation for a polar angle of 40° in this case. The two cases are correlated, with the azimuth of minimum attenuation corresponding to the azimuth of highest velocity. This azimuth lies at 110°, midway between the strike directions of the two fracture sets.

An interesting case is one in which two sets of fractures exist but only one set supports fluid communication with the matrix. The noncommunicating set may be sealed for many reasons, including mineral filling or the imposition of unequal horizontal stress. This case can be modeled by allowing the timescale constant for the sealed set to approach infinity, corresponding to a vanishing permeability for exchange of fluid for those fractures.

We now seal the fracture set striking at 130°. In this case, both fracture sets result in directional variation of velocity, but only the open set produces attenuation and dispersion. Figure 4 shows the azimuthal variation of P-wave velocity and attenuation. This time, the minimum attenuation direction is 90°, corresponding to the strike direction of the open fracture set, but the direction of maximum velocity (around 100°) is a weighted average of the two strike directions. This suggests that azimuthal permeability on a larger scale, which is expected to be influenced more greatly by the communicating fractures, could be related more closely to attenuation anisotropy than to velocity anisotropy.

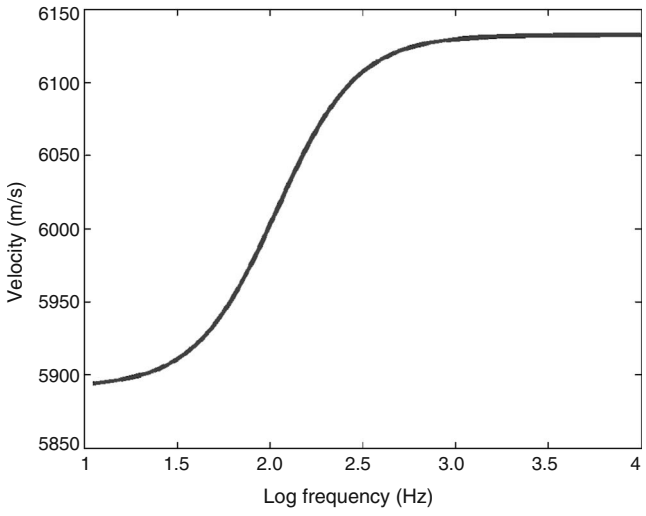

Figure 1. P-wave velocity as a function of frequency for 10-cm fractures, and propagation with polar and azimuthal angles of 30°. Matrix properties are for calcite. Porosity is assumed to be 8%. The rock is considered to be water saturated.

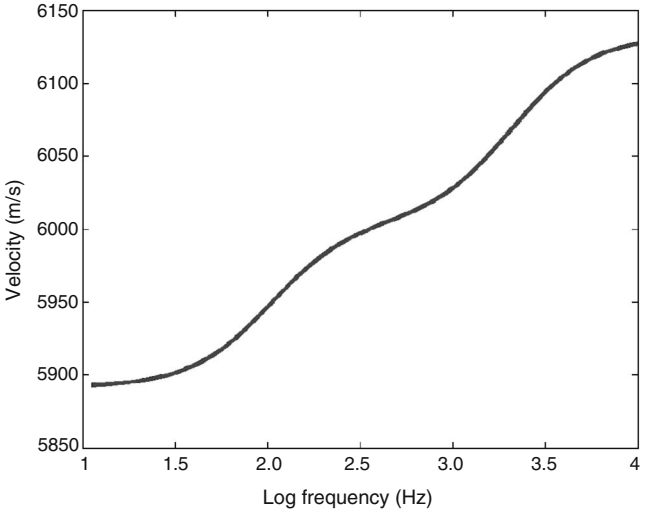

Figure 2. P-wave velocity as a function of frequency for two aligned fractures sets of 10-cm and 5-mm radii for propagation with polar and azimuthal angles of 30°. The other properties are the same as Figure 1.

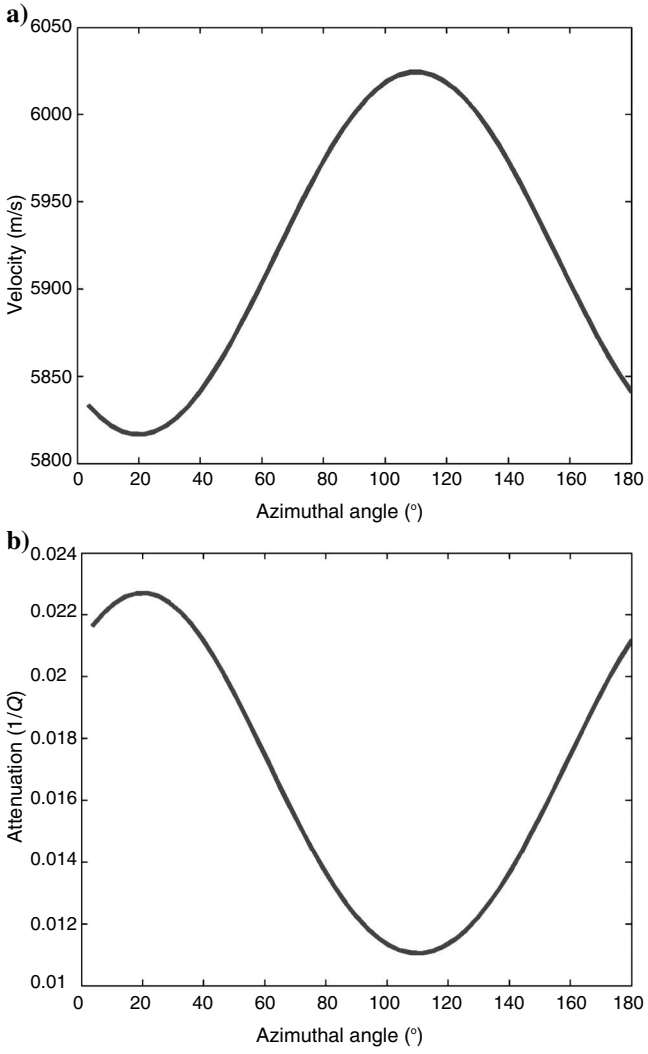

Figure 3. Azimuthal variation of (a) velocity and (b) attenuation for a polar angle of 40° for a medium with two identical fracture sets striking at 90° and 130°. The azimuth of maximum velocity coincides with that of minimum attenuation around 110°.

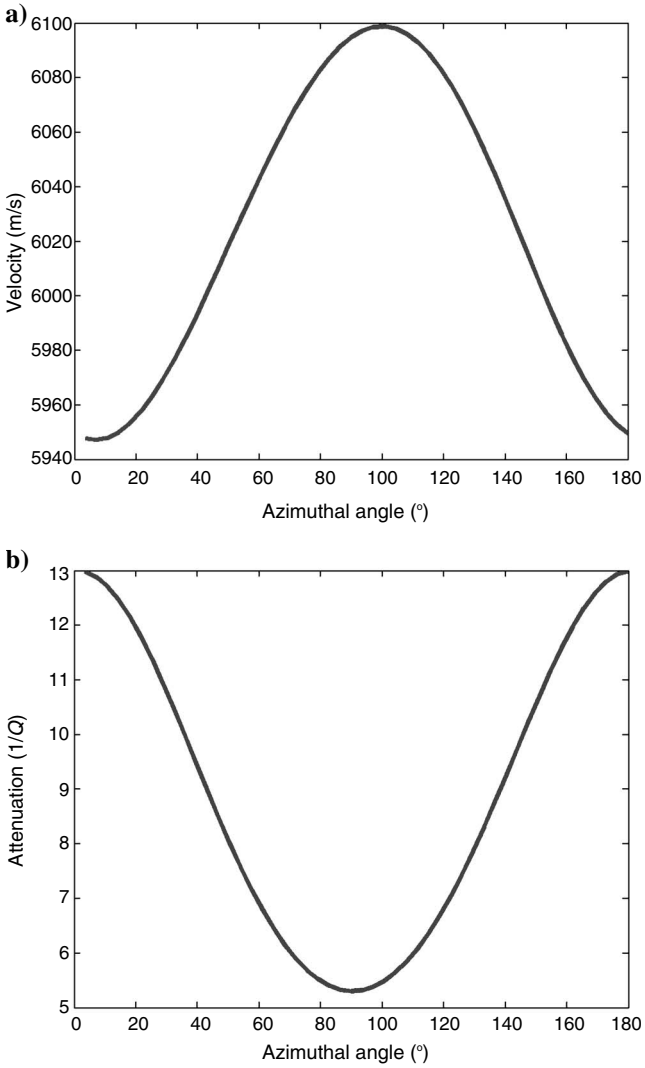

Figure 4. Azimuthal variation of (a) velocity and (b) attenuation for a polar angle of 40° for a medium with an open fracture set striking at 90° and a sealed fracture set striking at 130°. In this case, minimum attenuation occurs at an azimuth of 90° but maximum velocity is around 100°.

DISCUSSION

This study emphasises that anisotropic dispersion and attenuation may be expected theoretically in the seismic frequency band for wave propagation in fractured reservoirs. The frequency dependence of the anisotropy is controlled by two timescale parameters that are sensitive to the fracture scale lengths and fluid mobility.

I expect the results of this study to support current attempts to develop the interpretation of frequency-dependent anisotropy for improved fracture and fluid characterization. In particular, it supports the contention of Liu et al. (2007) that attenuation anisotropy is influenced strongly by the presence of open fractures and that traveltime anisotropy is controlled by a combination of open and closed fractures. Maultzsch et al. (2007b) present an analysis of multiazimuth VSP data that appears to show a link between attenuation anisotropy and the strike direction of open fractures.

The implicit reliance of the frequency dependence on fluid mobility raises the possibility that anisotropic attributes may be sensitive to fluid viscosity. Although some of the predicted effects may be subtle and hard to detect without sufficient azimuthal coverage, the contrast in viscosity between, for example, oil and water can be strong, and this can give rise to significant observable effects. This possibility emphasizes the importance of careful rock-physics modeling when we deal with reservoirs with complex fracture patterns.

CONCLUSIONS

My technique allows one to model the effect of two fracture sets of different sizes, orientations, and connectivities on the anisotropic response of porous rock. The results generalize those of earlier work that was restricted to a single set of fractures. The current technique is valid to the first order in the number density of the fractures.

In this case, the behavior is influenced by two characteristic frequencies, or timescale parameters, corresponding to the two length scales of the fractures. This implies that dispersion and attenuation can occur over a wider frequency band than is possible in the single-scale case. When the two fracture sets have different connectivities,

the attenuation anisotropy and velocity anisotropy can be very different. Thus, it may be possible to use such measurements to distinguish between open and closed fractures.

ACKNOWLEDGMENTS

The author thanks Enru Liu and Morten Jakobsen for many discussions on this topic. The paper was improved by a number of anonymous reviewers. This work is supported by the sponsors of the Edinburgh Anisotropy Project and is published with the permission of the Executive Director of the British Geological Survey (NERC).

REFERENCES

Barton, N., 2007, Rock quality, seismic velocity, attenuation and anisotropy: Taylor and Francis.

Batzle, M. L., D. H. Han, and R. Hoffmann, 2006, Fluid mobility and frequency-dependent seismic velocity — Direct measurements: Geophysics, **71**, no. 1, N1–N9.

Chapman, M., 2003, Frequency-dependent anisotropy due to meso-scale fractures in the presence of equant porosity: Geophysical Prospecting, **51**, 369–379.

Chapman, M., S. V. Zatsepin, and S. Crampin, 2002, Derivation of a microstructural poroelastic model: Geophysical Journal International, **151**, 427–451.

Eshelby, J. D., 1957, The determination of the elastic field of an ellipsoidal inclusion, and related problems: Proceedings of the Royal Society of London A, **241**, 376–396.

Hudson, J. A., E. Liu, and S. Crampin, 1996, The mechanical properties of materials with interconnected cracks and pores: Geophysical Journal International, **124**, 105–112.

Jakobsen, M., 2004, The interacting inclusion model of wave induced fluid flow: Geophysical Journal International, **158**, 1168–1176.

Liu, E., M. Chapman, I. Varela, X.-Y. Li, J. H. Queen, and H. B. Lynn, 2007, Velocity and attenuation anisotropy: Implication of fracture characterizations: The Leading Edge, **26**, 1170–1175.

Maultzsch, S., M. Chapman, E. Liu, and X.-Y. Li, 2007a, Observation of anisotropic attenuation in VSP data: Journal of Seismic Exploration, **16**, no. 2–4, 145–158.

———, 2007b, Modeling and analysis of attenuation anisotropy in multiazimuth VSP data from the Clair field: Geophysical Prospecting, **55**, 627–642.

Pointer, T., E. Liu, and J. A. Hudson, 1996, Seismic wave propagation in cracked porous media: Geophysical Journal International, **142**, 199–231.

van der Kolk, C. M., W. S. Guest, and J. H. H. M. Potters, 2001, The 3D shear experiment over Natih field in Oman: The effect of fracture-filling fluids on shear propagation: Geophysical Prospecting, **49**, 179–197.